JOURNAL OF AIRCRAFT
Vol. 34, No. 4, July–August 1997

Experimental Investigation of Semispan Model Testing Techniques

Gregory M. Gatlin* and Robert J. McGhee†
NASA Langley Research Center, Hampton, Virginia 23681-0001

An investigation has been conducted in the NASA Langley Research Center's 14 by 22 ft Subsonic Tunnel to further the development of semispan testing capabilities. A twin-engine, energy efficient transport model with a four-element wing in a takeoff configuration was used for this investigation. Initially, a full-span configuration was tested, and force and moment data and wing and fuselage surface pressure data were obtained as a baseline data set. The semispan configurations were then mounted on the wind-tunnel floor, and the effects of fuselage standoff height and shape were investigated. Results indicate that the semispan configuration was sensitive to variations in standoff height, and that a standoff height equivalent to 30% of the fuselage radius resulted in better correlation with full-span data than no standoff or the larger standoff configurations investigated. Undercut standoff leading edges improved the correlation of semispan data with full span data in the region of maximum lift coefficient.

Nomenclature

b = wingspan, in.
C_D = drag coefficient
C_L = lift coefficient
C_M = pitching-moment coefficient
C_p = pressure coefficient
d = fuselage diameter, in.
M = Mach number
Re_n = Reynolds number based on mean geometric chord
y = spanwise location, in.
x/c = longitudinal distance from airfoil leading edge nondimensionalized by local wing chord
x/L = longitudinal distance from fuselage nose nondimensionalized by fuselage length
α = angle of attack, deg

Introduction

GENERALLY in most types of wind-tunnel testing, research requirements dictate that the most accurate data be obtained and that the correct flight conditions be simulated. These issues are increasingly important to develop accurate performance characteristics, particularly at the low-speed takeoff and approach conditions encountered by subsonic transport aircraft. Typically the Reynolds numbers achievable at the speeds appropriate for takeoff and approach conditions in the current facilities available are well below the desired full-scale Reynolds number. This need to extend Reynolds number testing capabilities up to full-scale conditions can be satisfied with the development of a semispan testing capability. This testing technique has been suggested as a tool that should be developed to provide state-of-the-art wind-tunnel research capabilities.[1,2]

Semispan testing offers several advantages over full-span testing. Because of the larger model size provided by semispan testing, not only is the desired increased Reynolds number testing capability produced, but the larger model size also improves data quality because of improved model strength, stiffness, and overall fidelity. Constructing only half the model yields further benefits in terms of reduced model cost. The complex high-lift systems and any wing-mounted propulsion simulation systems will only need to be produced for one wing. Another advantage of semispan testing is the absence of sting-support interference effects. Semispan testing, however, does have its disadvantages. These include increased wind-tunnel wall interference effects caused by increased model size and the effects of semispan model mounting. One of the most significant challenges is how to remove the effects of the tunnel wall boundary layer on the flow over the semispan model. These adverse effects include loss of model symmetry, wall boundary-layer separation, and the formation of vortical flow in the juncture regions. Research previously conducted[3] indicates that even when the wall boundary layer remains attached it can still substantially influence the flow over the semispan model. One technique that has been investigated to isolate the effects of the wall boundary layer is to mount the semispan model on a splitter plate that is offset from the tunnel wall outside the wall boundary layer. This technique certainly minimizes any wall boundary-layer effects; however, it introduces difficulties in maintaining a uniform flow over the model without introducing any undesirable flow angularity. These issues can be overcome, but generally at the expense of a substantial calibration effort.[4] Results from previous semispan testing technique studies have generally been more promising when a nonmetric boundary-layer standoff is used between the semispan model and the wind-tunnel wall.[4–6]

To further understand the flow physics involved in semispan testing as well as to develop techniques to eliminate or minimize the effects of the wall boundary layer, both computational methods[7] and experimental studies have been utilized. A wind-tunnel investigation has been conducted in the NASA Langley Research Center's 14 by 22 ft Subsonic Tunnel using both a full-span and a semispan transport model with a four-element wing in a takeoff configuration. The full-span configuration was tested initially, and force and moment data and wing and fuselage surface pressure data were obtained as a baseline data set. The semispan configurations, which were designed to use a floor mount and a nonmetric boundary-layer standoff, were then tested to study the effects of standoff height and

Presented as Paper 96-2386 at the AIAA 14th Applied Aerodynamics Conference, New Orleans, LA, June 17–20, 1996; received Sept. 29, 1996; revision received March 10, 1997; accepted for publication March 14, 1997.

*Research Scientist, Subsonic Aerodynamics Branch, Aero- and Gas-Dynamics Division. Senior Member AIAA.

†Research Scientist, Subsonic Aerodynamics Branch, Aero- and Gas-Dynamics Division.

shape. The criteria used to determine the effectiveness of a given standoff geometry were simply to assess how well the force and moment and pressure data from the semispan configuration compared with that of the full-span configuration. It is the results of these investigations that will be presented in this paper.

Test Facility and Model Description

The investigation was conducted in the NASA Langley Research Center's 14 by 22 ft Subsonic Tunnel.[8] This facility is a closed-circuit, single-return, atmospheric wind tunnel capable of producing a maximum speed of 338 fps. A floor boundary-layer removal system is located at the entrance to the test section and was used in the current investigation to reduce the size of the floor boundary layer to a minimum height of 2 in. at the semispan model location.

The model used in the investigation was a 10.59-ft span, unpowered, twin-engine transport known as the energy efficient transport (EET) configuration. The full-span model (Fig. 1) was tested first to provide a baseline database. The fuselage was 9.91 ft long and had a maximum diameter of 13.8 in. The wing had an aspect ratio of 10, a leading-edge sweep of 28.8 deg, and employed a supercritical airfoil with a four-element high-lift system consisting of a slat, main element, vane, and flap. All of the results presented in this paper are for a takeoff configuration with the slats deflected −50 deg, the vanes 15 deg, and the flaps 30 deg. These deflection angles are all with respect to the main wing element. Pressure instrumentation was located on the wing and fuselage as illustrated in Fig. 1. The full-span model was mounted on a six-component strain-gauge balance and supported by a sting that entered the lower aft end of the fuselage. No vertical or horizontal tails were used in the investigation. A wing reference area and reference geometric chord of 11.21 ft^2 and 13.44 in., respectively, were used in the calculations of the force and moment coefficients.

The semispan model consisted of the port wing from the full-span model and a semifuselage that was fabricated from a mold of the full-span fuselage. In addition, all semispan configurations were tested with a simulated sting. These steps were taken to ensure that no geometric differences would exist between the full-span and semispan configurations. A photograph of the semispan model installation in the wind tunnel is presented in Fig. 2. The model was mounted on a 15.75-ft-diam turntable on the floor of the tunnel approximately 6 ft aft

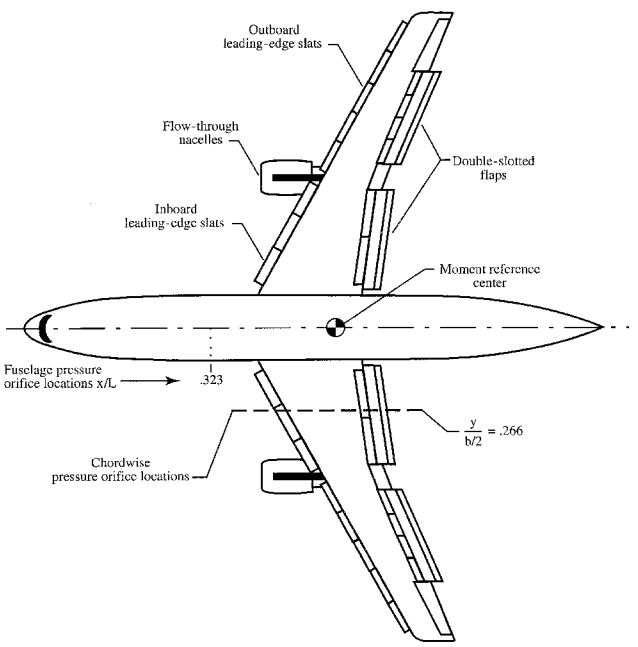

Fig. 1 Full-span EET model in the takeoff configuration.

Fig. 2 Semispan EET model as tested with the 2-in., two-dimensional standoff in the 14 by 22 ft Subsonic Tunnel.

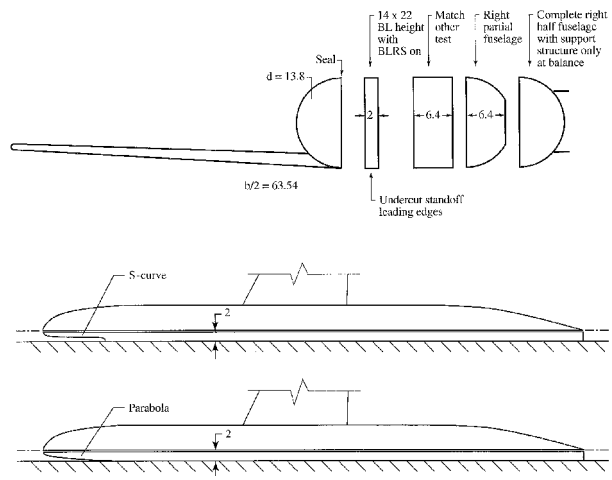

Fig. 3 Standoff geometries tested on the semispan model. All dimensions are in inches: a) cross-sectional views of the standoff geometries and b) top-view illustrations of the undercut leading edges tested on the 2-in. standoff. (BL, boundary layer.)

of the tunnel floor boundary-layer removal system (BLRS). A six-component strain-gauge balance was used to measure forces and moments on the wing and semifuselage. All standoffs, however, were nonmetric. A polyurethane foam seal was used around the perimeter of the fuselage to fill the 0.25-in. gap between the fuselage and the standoff so that no freestream flow would enter this region. This seal was carefully installed during each standoff installation to ensure that no fouling would occur between the metric fuselage and the nonmetric standoffs. All standoffs were attached to the tunnel floor and sealed such that no freestream flow could pass between the standoff and the floor. The semispan model was tested with no standoff, and 2- and 6.4-in. two-dimensional (2-D) standoffs. These standoffs were the same shape as the perimeter centerline shape of the fuselage. Additionally, a three-dimensional (3-D), 6.4-in. standoff that was a mirror image of the semifuselage and a complete right side of the fuselage were tested. All of these standoff shapes are presented in Fig. 3a. Further tests were conducted in which three-dimensionally shaped undercut leading edges were tested on the 2-in. standoff configuration. Illustrations of these undercut leading edges are presented in Fig. 3b.

Test Conditions and Techniques

All testing for both the full-span and semispan configurations was conducted at $M = 0.20$, $Re_n = 1.6 \times 10^6$, and over

an angle-of-attack range of −4 to 24 deg. The moment reference center was located on the fuselage centerline 64.70 in. back from the nose on both the full-span and semispan configurations. Transition grit was placed on the fuselage nose and on the nacelles, but not on any of the wing elements for both configurations. Base pressure corrections were applied to the full-span configuration to account for the effects of the sting entering the lower aft end of the fuselage. A simulated sting was positioned external to the semispan configuration to generate the same flowfield encountered by the full-span configuration. Since the simulated sting did not enter the semispan fuselage, no base pressure corrections were applied. A simulated semisting was used for the no standoff and 2-in. standoff configurations (see Fig. 2). A simulated full sting was used for all configurations with a larger standoff. For all semispan configurations investigated the simulated sting was adjusted up or down to accommodate the height of the current standoff. Model blockage corrections and jet boundary corrections were applied in the same manner to both full-span and semispan configurations. A flow angularity correction was also applied to both configurations (0.141-deg upflow for the full-span model and 0.081-deg downflow for the semispan model). The wind-tunnel BLRS was used for all semispan data presented in this paper. The use of the BLRS reduced the boundary layer on the floor of the wind tunnel to a minimum height of 2 in. at the moment reference center of the model. Surface flow visualization images were obtained of the wind-tunnel floor around the semispan configuration using an oil-based mixture consisting of mineral oil, oleic acid, and titanium dioxide. Flow visualization images were obtained of the upper surface of the wing for both full-span and semispan configurations using fluorescent minitufts, ultraviolet strobe lights, and a video imaging system. An assessment of data accuracy indicates that for the full-span configuration the coefficient data presented have an error no greater than ± 0.006 for C_L, ± 0.0030 for C_D, and ± 0.0039 for C_M. For the semispan configuration the errors are no greater than ± 0.012 for C_L, ± 0.0075 for C_D, and ± 0.0083 for C_M. For both full- and semispan configurations, the pressure coefficient data have errors no greater than ± 0.007. These error bands were determined based on the accuracies of the instrumentation used and verified via multiple repeat runs.

Discussion

Standoff Height Effects

One of the primary goals of this investigation was to determine the effects of variations in standoff height. The first step in this process was to investigate height variation using a two-dimensionally shaped standoff. To do this the semispan configuration was tested with no standoff, a 2-in. standoff, and a 6.4-in. standoff. The no-standoff configuration was chosen as the obvious case to represent the minimum standoff height. The 2-in. height, which was equal to approximately 30% of the fuselage radius, was chosen because it corresponds to the height of the floor boundary layer at the model moment reference center with the BLRS on. The 6.4-in. height, which was equal to approximately 93% of the fuselage radius, was chosen because it provided a direct comparison to a standoff height that was previously investigated on a smaller-scale EET model in another facility. It was further believed that the 6.4-in. height represented a reasonable maximum height and that a two-dimensional standoff that was any taller would produce no benefit. This standoff height is equivalent to about three times the floor boundary-layer thickness with the BLRS on and was expected to result in large effects. The results obtained from these configurations are presented together for comparison in Fig. 4. The force and moment data indicate that for angles of attack up to 12 deg, the configuration with the 2-in. standoff correlates better with full-span data in terms of lift, lift−curve slope, and drag coefficient than the other standoff

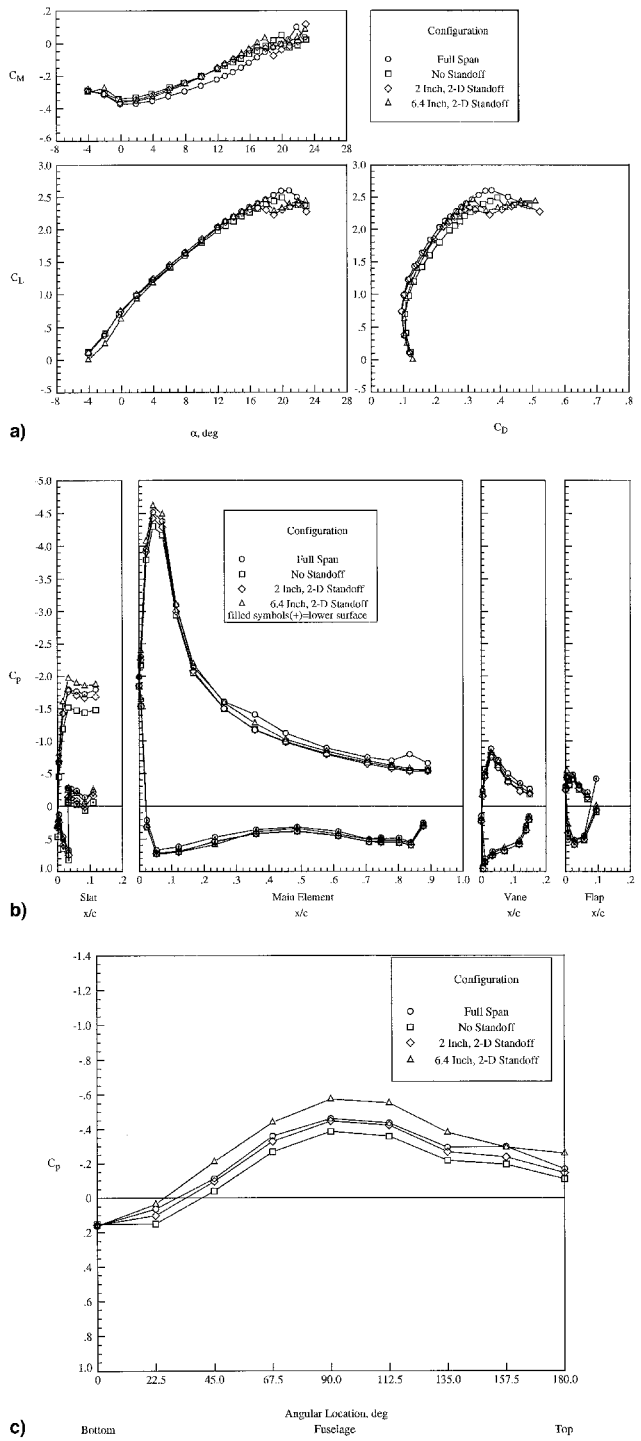

Fig. 4 Data illustrating the effects of variations in two-dimensional standoff height: a) longitudinal force and moment data, b) wing pressure data (α = 16 deg), and c) fuselage pressure data (x/L = 0.323, α = 16 deg).

configurations. The no-standoff configuration results in a reduced lift−curve slope and a substantial drag increase, whereas the larger standoff indicates an increase in lift−curve slope and a drag increase. Collectively, these data indicate that increases in two-dimensional standoff height produce increases in lift−curve slope. The 2-in. standoff configuration however, produces a stall angle of attack that is approximately 4 deg less than that of the full-span configuration. It is also noted that the no-standoff configuration comes closest to matching the stall angle of attack while the other configurations stall early. None of the standoff configurations produced a very good cor-

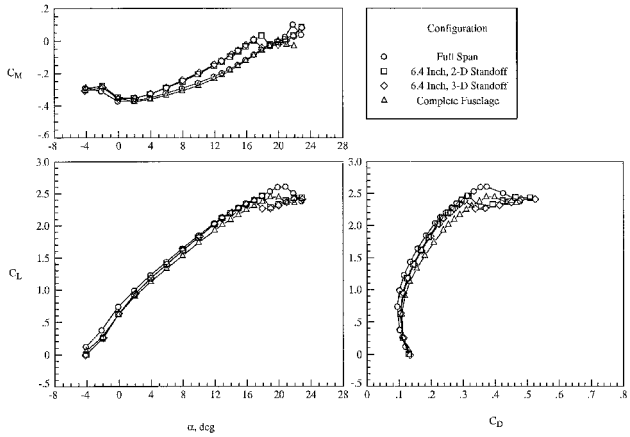

Fig. 5 Longitudinal force and moment data illustrating the effects of the larger, mirror-image standoffs.

relation with the full-span configuration in terms of pitching moment. For the nonzero standoff configurations this could be because of a slight misalignment between the fuselage and standoff caused by balance deflections.

Pressure data presented for the inboard portion of the wing (Fig. 4b) indicate that at 16-deg angle-of-attack flow conditions on the slat and the leading edge of the main element correlate better with the full-span data for the 2-in. standoff configuration than the other two standoff configurations. In fact, a trend is indicated that shows a flow acceleration over the slat and the main element leading edge as standoff height is increased. This could lead to the conclusion that increases in standoff height produce increases in the flow acceleration around the fuselage, which in turn produce the flow accelerations noted on the wing leading edge. When fuselage pressure data are compared for the various standoff configurations (Fig. 4c), it is shown that increases in standoff height do indeed produce increases in the flow acceleration around the fuselage. These data also further support the conclusion that the 2-in. standoff configuration more accurately simulates the full-span configuration than the other standoff geometries.

Two additional standoff configurations were also tested as a part of this investigation: 1) a three-dimensionally shaped 6.4-in. standoff that was a mirror image of the semifuselage and 2) a complete right side of the fuselage. It was anticipated that the size, which would offset the model farther from the tunnel floor, along with the three-dimensional shaping of these standoffs may act to reduce the effects of the floor boundary layer on the semispan configurations. Force and moment data obtained for these additional standoff configurations are presented in Fig. 5. Lift losses and drag increases are noted for both configurations when compared to the full-span data. More specifically, the 6.4-in., three-dimensional standoff shows no improvement over the 6.4-in., two-dimensional standoff, and the configuration with the complete fuselage produces the largest lift deficit and largest drag increase of all standoffs investigated. Even though the configuration with the complete fuselage shows good correlation with full-span data in terms of pitching moment, the poor lift and drag correlation are still viewed as substantial drawbacks. Since these larger, mirror-image standoffs did not result in an overall improvement in correlation with full-span data they were given no further consideration. Based on all of the semispan data presented thus far, the overall results indicate that semispan configuration aerodynamics are quite sensitive to variations in standoff height.

Undercut Standoff Leading-Edge Effects

When any two-dimensional standoff is used, it is understood that a stagnation point will exist at some location on the leading edge. This stagnation point causes the freestream flow to roll up on itself in the floor boundary layer, and a horseshoe vortex will form around the standoff leading edge. To document and illustrate this flow condition, a surface oil flow pattern was obtained on the tunnel floor for the 2-in., two-dimensional standoff configuration. This oil flow pattern, presented in Fig. 6 for an angle of attack of 19 deg, gives an indication of the horseshoe vortex size and location.

It was anticipated that the presence of a horseshoe vortex around the leading edge of a two-dimensional standoff was detrimental to efforts to match the flowfield around a full-span configuration. With this thought in mind two undercut leading edges as illustrated in Fig. 3b were tested on the 2-in. standoff. These undercut shapes are referred to as an S-curve leading edge and a parabola leading edge. The S-curve leading edge was designed using computational methods such that a favorable pressure distribution would result in the cockpit region of the forebody. The parabola leading edge was designed such that no forward-facing surfaces would exist, thereby resulting in a geometry that would make it much more difficult for a horseshoe vortex to form. Longitudinal force and moment data illustrating the effects of the standoff undercut leading edges are presented in Fig. 7a. These data indicate that undercut standoff leading edges have essentially no effect on lift–curve slope, but have a significant effect on the stall angle of attack. The S-curve leading edge increases the stall angle of attack by approximately 2 deg over the two-dimensional configuration, and the parabola leading edge increases the stall angle of attack by approximately 3 deg. These results thereby suggest that the elimination or reduction in size of the horseshoe vortex will improve correlation of semispan and full-span data in the region of maximum lift coefficient. This point is further supported upon re-examination of the lift coefficient data presented for the no-standoff configuration in Fig. 4a. Even though the no-standoff configuration does not correlate well with full-span data across the angle-of-attack range, it does match the stall angle of attack much better than the other two-dimensional standoff configurations. This may well be because it is much more difficult for a horseshoe vortex to form on the no-standoff configuration.

Even though the undercut standoff leading edges do improve the correlation of stall angle of attack and maximum lift coefficient with full-span data, they are not without shortcomings. The undercut leading edges result in an increase in drag as compared to the two-dimensional leading edge, and the reason for this unfavorable characteristic is unknown. As a result a more thorough understanding of the flow physics will be pursued through computational and experimental efforts. Examination of the pitching-moment data reveals a nose-down increment beyond the stall angle of attack for all of the semispan configurations. This indicates that wing stall begins on

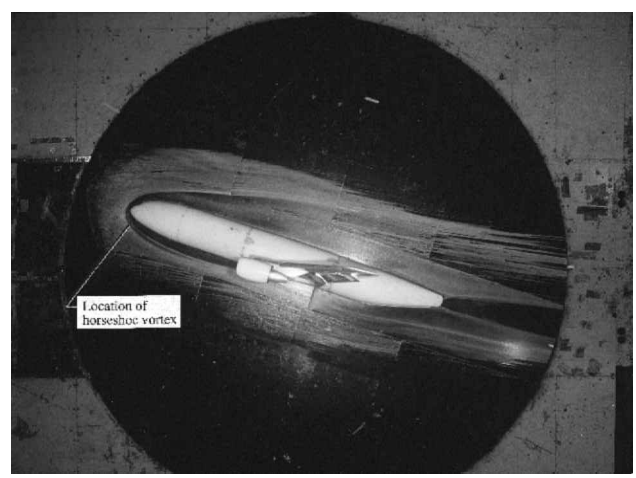

Fig. 6 Oil flow visualization illustrating surface flow characteristics on the tunnel floor for the 2-in., two-dimensional standoff configuration (α = 19 deg).

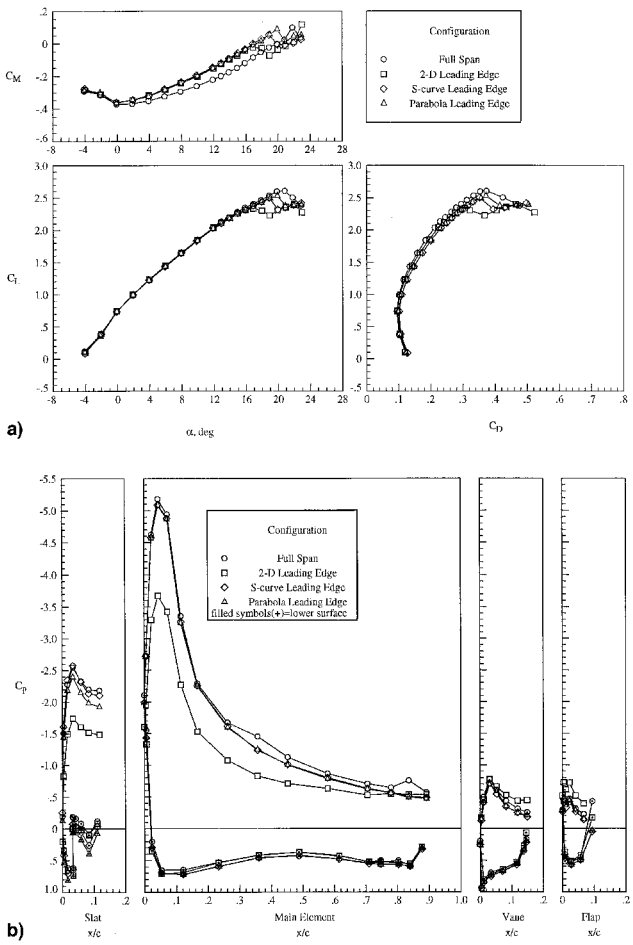

Fig. 7 Data illustrating the effects of undercut leading edges on the 2-in. standoff configuration: a) longitudinal force and moment data and b) wing pressure data (α = 19 deg).

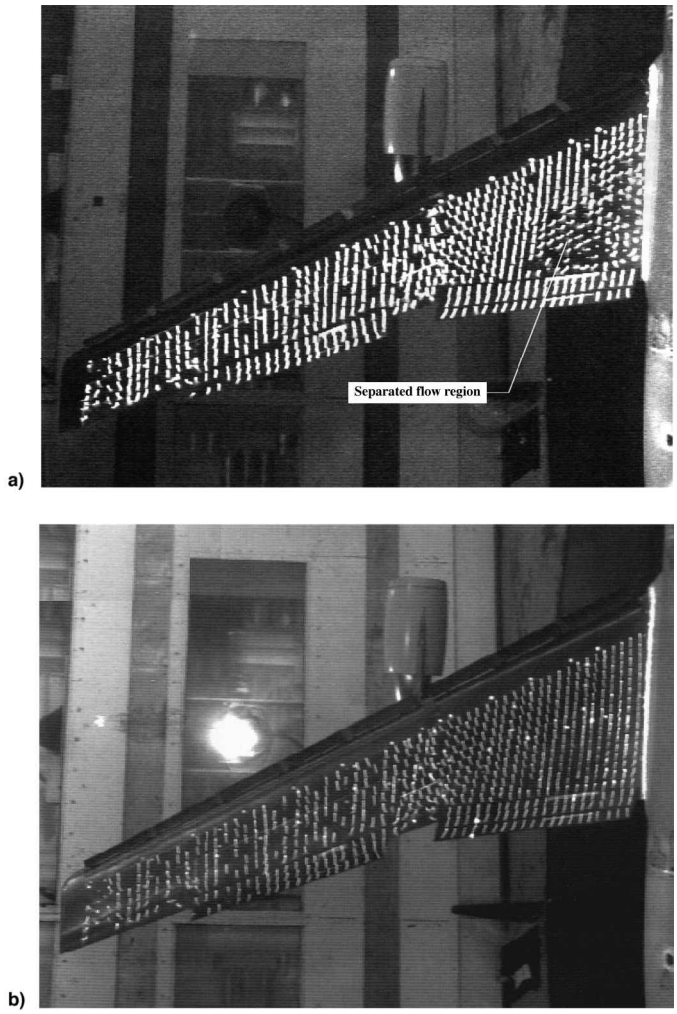

Fig. 8 Flow visualization illustrating wing upper surface flow characteristics with 2-inch standoff (α = 19 deg): a) two-dimensional and b) S-curve standoff leading edges.

the inboard portion of the wing. This does not match the post-stall nose-up increment indicated by the full-span data. This inconsistency has also been noted in previous research.[6] The fact that the stall behavior on the semispan configurations with undercut standoff leading edges does not match that on the full-span model indicates that the influence of the floor boundary layer on the flowfield over the wing may still not be fully eliminated. Inboard wing pressure data are presented for an angle of attack of 19 deg in Fig. 7b to further illustrate the effects of the undercut standoff leading edges. These data indicate that the configuration with the two-dimensional standoff leading edge is producing less lift on the slat and main element than the undercut standoff configurations, whereas the data from the undercut configurations match the full-span data relatively well. These data further support the inboard wing stall noted in the discussion of the pitching-moment data.

Further insight into the flow conditions on the wing upper surface was obtained through the use of flow visualization. Fluorescent minituft images of the wing upper surface have been obtained for configurations with the two-dimensional standoff leading edge and the S-curve leading edge, and these images are presented for an angle of attack of 19 deg in Fig. 8. A region of separated flow is indicated inboard on the wing for the configuration with the two-dimensional standoff leading edge (Fig. 8a), as would generally be expected because of the wing pressure data presented in the previous figure. The image of the wing for the configuration with the S-curve leading edge (Fig. 8b) indicates smooth, attached flow over the entire inboard portion of the wing. These results suggest that the horseshoe vortex that forms around the leading edge of the two-dimensional standoff produces an undesirable flow disturbance that ultimately affects the flow over the inboard portion of the wing. This disturbance promotes an inboard wing stall and resulting nose-down pitching moment. The undercut leading-edge configurations ultimately stall in the same fashion; however, the leading-edge undercut shaping appears to be effective in delaying the onset of the flow disturbances that produce the inboard wing stall.

Conclusions

An investigation has been conducted in the NASA Langley Research Center's 14 by 22 ft Subsonic Tunnel where a semispan transport configuration has been tested with multiple parametric variations to support the development of a viable semispan testing technique. The results of this investigation are presented as follows:

1) The semispan transport configuration investigated demonstrated a sensitivity to variations in standoff height. Increases in standoff height resulted in increased flow acceleration around the fuselage and over the inboard wing leading edge.

2) Configurations with no standoff produced a reduction in lift–curve slope and more drag than the baseline full-span configuration.

3) Configurations with standoff heights on the order of the fuselage radius produced an increase in lift–curve slope and drag compared to the baseline full-span configuration.

4) A 2-in. standoff, which was equal to approximately 30% of the fuselage radius, produced the best correlation with full-

span data for angles of attack below 12 deg of all the standoff configurations tested.

5) A two-dimensional standoff leading edge promotes the formation of a horseshoe vortex in the standoff/floor juncture and in turn promotes an early inboard wing stall.

6) The early inboard wing stall that occurred with the two-dimensional, 2-in. standoff was effectively delayed by an undercut standoff leading edge.

References

[1]Lynch, F. T., "Experimental Necessities for Subsonic Transport Configuration Development," AIAA Paper 92-0158, Jan. 1992.

[2]Viehweger, G., and Ewald, B., "Half Model Testing in the Cologne Cryogenic Tunnel (KKK)," AIAA Paper 94-2511, June 1994.

[3]Milholen, W. E., II, and Chokani, N., "Effect of Sidewall Boundary Layer on Transonic Flow over a Wing," *Journal of Aircraft*, Vol. 31, No. 4, 1994, pp. 986–988.

[4]Franz, H. P., "The Half-Model Technique in the Wind Tunnel and Its Employment in the Development of the Airbus Family," NASA TM-76970, Aug. 1982 (Translation of DGLR Paper 81-118).

[5]Boersen, S. J., "Half-Model Testing in the NLR High-Speed Wind Tunnel HST, a 1981 Status Report," National Aerospace Lab., TR 82123U, Aug. 1982.

[6]Earnshaw, P. B., Green, A. R., Hardy, B. C., and Jelly, A. H., "A Study of the Use of Half-Models in High-Lift Wind-Tunnel Testing," CP-515, AGARD, Oct. 1992, pp. 20.1–20.9.

[7]Milholen, W. E., II, Chokani, N., and McGhee, R. J., "Development of Semi-Span Model Test Techniques," AIAA Paper 96-2412, June 1996.

[8]Gentry, G. L., Jr., Quinto, P. F., Gatlin, G. M., and Applin, Z. T., "The Langley 14- by 22-Foot Subsonic Tunnel: Description, Flow Characteristics, and Guide for Users," NASA TP-3008, Sept. 1990.